Thermodynamics of the unitary Fermi gas

Olga Goulko[*]

Ludwig-Maximilians-University, Faculty of Physics, Chair of Theoretical Solid State Physics,
Theresienstr. 37, 80333 Munich, Germany
E-mail: `O.Goulko@physik.uni-muenchen.de`

M. Wingate

DAMTP, University of Cambridge, Wilberforce Road, Cambridge CB3 0WA, UK
E-mail: `M.Wingate@damtp.cam.ac.uk`

Lattice field theory has become an increasingly popular method to study problems in the field of cold atoms. For strongly interacting systems, such as the unitary Fermi gas, a numerical simulation is often the only reliable tool to give quantitative predictions. In this work we build upon our previous calculation of the critical temperature of the unitary Fermi gas with the determinant diagrammatic Monte Carlo method. Now we generalise our approach to temperatures above and below the critical point and present results for the temperature dependence of the chemical potential, the energy per particle and the contact density. Our values show good agreement with recent experimental data.

---

[*]Speaker.

1. Introduction

In his talk "Simulating physics with computers" given at the First Conference on Physics and Computation [1], Richard Feynman addressed the question how to simulate a quantum mechanical system with the following proposition:

> *Let the computer itself be built of quantum mechanical elements which obey quantum mechanical laws.*

Such a universal quantum simulator is, to a certain extent, realised by a cold atomic gas, which can be created and studied experimentally. An atomic gas is dilute, such that the interparticle distances are large and the particles are essentially uncorrelated. At very low temperatures quantum mechanical phenomena become apparent. Hence cold atomic gases can provide a direct realisation of many basic models in condensed matter physics.

Dilute gases can be easily manipulated with lasers and magnetic fields, which gives experimentalists excellent control over many properties, such as interaction strength, temperature, trapping potential and even dimension. At low temperatures the thermal de Broglie wavelength is large compared to the range of the interatomic potential and the exact form of the interaction becomes unimportant for the macroscopic properties of the system. Therefore the model of a dilute quantum gas can represent various systems in nature and can be used in different areas of physics. For example it finds application in nuclear physics where results from the field of cold gases can be used to describe systems such as low-density neutron matter or even atomic nuclei. The neutrons in the core of a neutron star are believed to form a fermionic condensate that can be studied with the methods of cold Fermi gases. Even quantum chromodynamics at high temperatures and densities might have similar physics to these models.

Fermions are particularly interesting, since interactions between different spin states can result in a multitude of different regimes [2]. At low energies the dominant contribution comes from *s*-wave scattering which is governed by a single scale called the scattering length a. The regime of divergent scattering length $a \to \infty$ is called unitarity. The behaviour of the gas then only depends on two dimensionful parameters: the temperature and the density of the system. Hence all thermodynamic observables must be universal functions of the temperature T and the Fermi energy of the non-interacting gas $\varepsilon_F = (3\pi^2 n)^{2/3}/2m$. For instance the critical temperature is simply a dimensionless number times the Fermi energy, while the chemical potential in units of the Fermi energy is a purely universal function of the temperature.

Due to the nonperturbative nature of the problem numerical approaches are the only ones that can give reliable quantitative predictions about the properties of the Fermi gas in the unitarity limit. Unlike the analytical approximations they can start directly from first principles and model the system in a systematically improvable way. They provide quantitative results that can be compared directly with experimental data and can be used as a benchmark to test analytical methods. In previous work [3] we used the diagrammatic determinant Monte Carlo (DDMC) algorithm [4] to numerically determine the critical temperature T_c and thermodynamic properties of the unitary Fermi gas at $T = T_c$. Now we extend our study to temperatures above and below T_c. We study the temperature dependence of the chemical potential, the energy density and the contact density.

2. General setup

We consider equal-mass fermions of two species labeled by the spin index $\sigma = \{\uparrow,\downarrow\}$. The simplest lattice model for such a system is the Fermi-Hubbard model. Its Hamiltonian in the grand-canonical ensemble reads

$$H = \sum_{\mathbf{k},\sigma}(\varepsilon_{\mathbf{k}} - \mu_{\sigma})c_{\mathbf{k}\sigma}^{\dagger}c_{\mathbf{k}\sigma} + U\sum_{\mathbf{x}}c_{\mathbf{x}\uparrow}^{\dagger}c_{\mathbf{x}\uparrow}c_{\mathbf{x}\downarrow}^{\dagger}c_{\mathbf{x}\downarrow}, \tag{2.1}$$

where the first term corresponds to the kinetic part of the Hamiltonian H_{kin} and the second term to the interaction part H_{int}. The units are chosen such that $\hbar = k_B = 2m = 1$. We work on a 3d periodic lattice with L^3 sites and lattice spacing set to unity. The discrete dispersion relation reads $\varepsilon_{\mathbf{k}} = \frac{1}{m}\sum_{j=1}^{3}(1 - \cos k_j)$, μ_{σ} is the chemical potential and $c_{\mathbf{k}\sigma}^{\dagger}$ ($c_{\mathbf{k}\sigma}$) the time-dependent fermionic creation (annihilation) operator. The coupling constant $U < 0$ corresponding to attractive interaction can be tuned so that the scattering length becomes infinite. The corresponding value in the infinite volume limit is $U = -7.914$ which is the value we use throughout the calculation.

According to [5] the partition function for this model can be written as a series of products of two matrix determinants (one for each spin species) built of free finite-temperature Green's functions. If $\mu_{\uparrow} = \mu_{\downarrow} \equiv \mu$ the two determinants are identical, since the spin-dependce enters only via the chemical potential. Therefore all terms in the series are squares and hence positive, and the series can be used as a probability distribution for Monte Carlo sampling. In this work we will limit ourselves to this case of equal populations in the two species.

We set the physical scale via $\nu = nb^3$, where $\nu = \langle \sum_{\sigma} c_{\mathbf{x}\sigma}^{\dagger}c_{\mathbf{x}\sigma} \rangle$ is the dimensionless filling factor, n the particle density and b the lattice spacing. As mentioned above, due to universality all physical quantities are given in units of the Fermi energy: $\varepsilon_F = (3\pi^2\nu)^{2/3}$ expressed through lattice quantities. To extract the physical results we need to perform two limits: the thermodynamic limit to infinite system size and then the continuum limit to zero lattice spacing. The former will be discussed in detail below. For the continuum limit we vary the chemical potential such that the filling factor tends to zero. This is equivalent to $b \to 0$ since $b \propto \nu^{1/3}$. Assuming that discretization errors are analytic in b, leading order lattice corrections are linear in $\nu^{1/3}$.

A detailed description of our numerical setup is given in [3, 6, 7]. We use the determinant diagrammatic Monte Carlo algorithm as introduced in [4] with several modifications which increase the efficiency by reducing autocorrelation effects that are present in the original setup.

3. Generalisation to finite temperature

Our previous work [3] has been limited to observables calculated at the critical temperature T_c. To move away from the critical point we need a prescription how to fix the temperature at different filling factors. The order parameter enabled us to distinguish the lattice critical temperature for any given value of the lattice chemical potential. We will use this lattice critical temperature $T_c(\mu)$ as a benchmark to fix the temperature scale.

On the lattice an additional artificial length scale is introduced by the lattice spacing. The simplest approach to vary the temperature is to hold the lattice chemical potential fixed and to vary
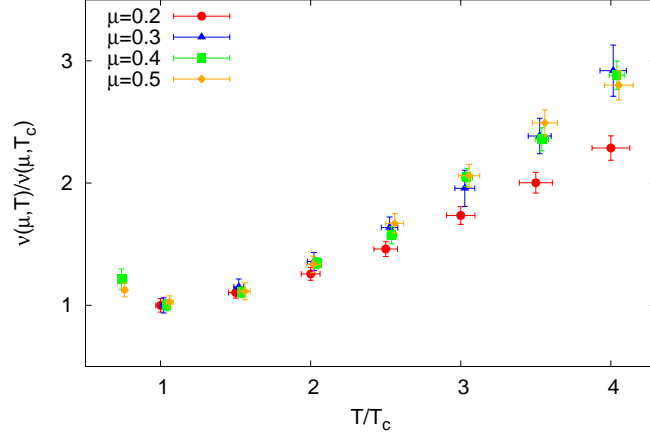
Figure 1: The normalised filling factor $\nu(\mu,T)/\nu(\mu,T_c)$ versus the temperature ratio T/T_c for different values of the lattice chemical potential μ. The values are horizontally offset for better comparison.

T. We set the lattice spacing such that it is independent of T,

$$b(\mu,T) = b(\mu,T_c) = \left(\frac{\nu(\mu,T_c)}{n(\mu,T_c)} \right)^{1/3}. \tag{3.1}$$

This can also be understood as a temperature-independent renormalisation condition. If we fix the lattice temperature ratio $r = T(\mu)/T_c(\mu)$ for each value of the lattice chemical potential, we will move along a line of constant temperature $T = rT_c$ and can perform a linear extrapolation towards the continuum. For coarse lattices this scheme will break down as the presence of the lattice spacing will change the relation between ν and T. To check for these lattice artefacts we consider the filling factor normalised by its value at the critical point, which must be independent of the lattice chemical potential, see Fig. 1. We observe that for sufficiently low temperatures $T \lesssim 3T_c$ the values of the filling factor are in good agreement with each other.

In the following we will study the temperature dependence of the chemical potential, the energy per particle and the contact density of the balanced unitary Fermi gas. We make these quantities dimensionless by scaling with appropriate powers of the Fermi energy $\varepsilon_F = k_F^2$. Data was taken below the critical temperature at $T/T_c = 0.7$ and for six different temperature ratios above the critical temperature, up to $T/T_c = 4$.

The continuum extrapolation is a linear fit of a dimensionless observable versus $\nu^{1/3}$. The filling factor ν can show finite-size effects. On small lattices we can expect a higher filling factor as a consequence of self-interactions due to boundary effects. In agreement with [4] we observe that the intercept of a linear fit of ν versus $1/L$ provides a good estimate for the thermodynamic limit of the filling factor. We performed simulations at several (usually three or four) values of lattice size L. The extrapolation $\nu(1/L \to 0)$ is used to obtain $\nu^{1/3}$ and ε_F in the thermodynamic limit. These quantities are then used for the continuum extrapolation.

3.1 Temperature dependence of the chemical potential

Figure 2 displays some of the numerical data for the chemical potential μ/ε_F at different tem-
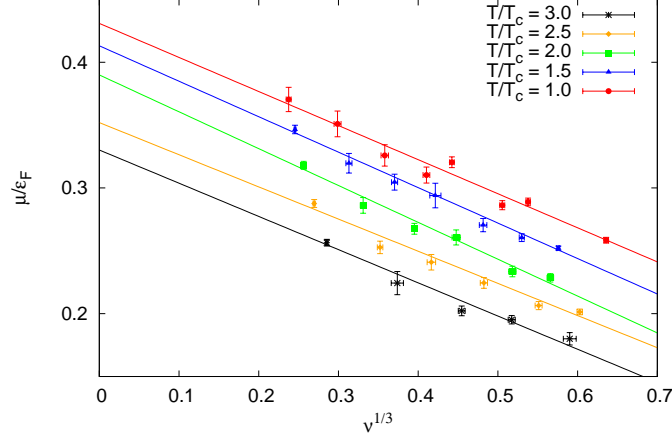
Figure 2: The chemical potential versus filling factor for different temperatures together with the linear fits. The continuum limit corresponds to $\nu \to 0$.

T/T_c	μ/ε_F	χ^2/d.o.f.	E/E_{FG}	χ^2/d.o.f.	$\mathscr{C}/\varepsilon_F^2$	χ^2/d.o.f.
4.0	0.266(6)	7.36	1.09(5)	0.39	0.116(4)	1.16
3.5	0.298(6)	3.47	1.11(5)	0.17	0.108(4)	1.68
3.0	0.330(7)	2.07	0.95(6)	2.48	0.103(4)	0.75
2.5	0.352(6)	2.69	0.90(4)	0.63	0.105(3)	1.56
2.0	0.390(6)	1.75	0.79(5)	0.33	0.100(3)	0.59
1.5	0.413(6)	0.93	0.82(4)	0.68	0.099(2)	0.28
1.0	0.431(8)	2.26	0.55(3)	0.46	0.114(4)	0.57
0.7	0.373(14)	0.85	0.41(5)	2.37	0.114(7)	0.24

Table 1: Continuum limit and goodness of fit for the chemical potential μ/ε_F, the energy density E/E_{FG} and the contact density $\mathscr{C}/\varepsilon_F^2$ at different temperatures.

peratures together with the linear continuum extrapolations. It is clearly visible that the chemical potential decreases with increasing temperature. A complete list of the fit results is given in Table 1. Figure 3 shows the continuum limit of the chemical potential as a function of the temperature. For temperatures $T \leq 2T_c$ we see excellent agreement with experimental data [8], as well as with several other theoretical predictions [9, 10]. In particular, our low-temperature value at $T = 0.7T_c$ correctly captures the experimentally observed change of the slope of the chemical potential curve. At high temperatures lattice artefacts become more pronounced and the results start to deviate.

3.2 Temperature dependence of the energy per particle

We express the energy per particle E/E_{FG} in units of $E_{\text{FG}} = (3/5)N\varepsilon_F$, which is the ground state energy of the free gas. The energy is composed of the kinetic energy E_{kin} and the interaction energy E_{int}. It can be shown [3] that on the lattice $E_{\text{kin}}/N = E_{\text{kin}}/L^3\nu$ can be expressed as

$$E_{\text{kin}}/L^3\nu = 6\left(1 - \frac{\sum_s \langle c_{\mathbf{x}s}^\dagger c_{(\mathbf{x}+\hat{\mathbf{j}})s}\rangle}{\nu}\right). \tag{3.2}$$
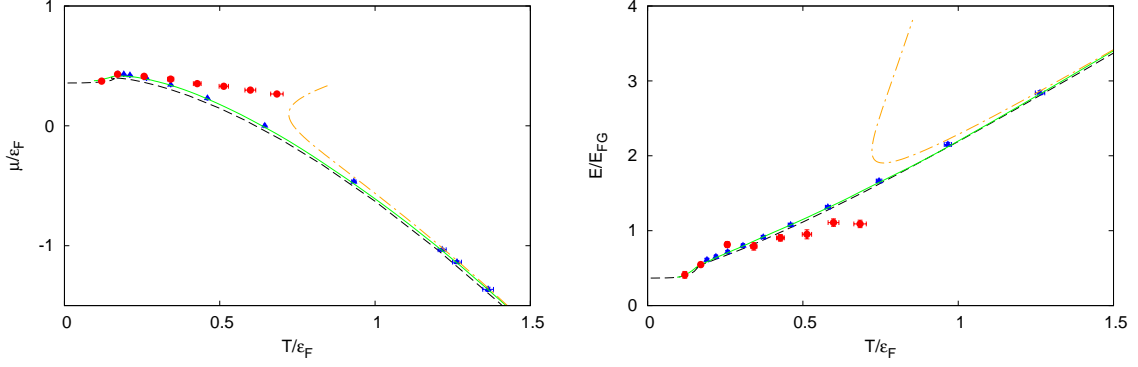
Figure 3: The chemical potential μ/ε_F (left) and the energy per particle (right) in the continuum limit versus the temperature T/ε_F. We compare our results (red circles) with experimental data [8] (green solid line), as well as results obtained with bold diagrammatic Monte Carlo [9] (blue triangles), the Luttinger-Ward formalism [10] (black dashed line), and the third order virial expansion [11] (orange dot dashed line).

From the structure of this equation it is evident that E_{kin}/N can have no dependence on the lattice size L. The same holds for interaction part of the energy. Therefore it is sufficient to consider the finite-size scaling of $1/\varepsilon_F$ (which follows directly from the finite-size scaling of ν), while the values of $E_{\mathrm{kin}}/L^3\nu$ obtained at different lattice sizes can simply be averaged. Our data confirms this, since the fits of $E_{\mathrm{kin}}/L^3\nu$ to a constant always yield acceptable χ^2-values.

The results for the continuum limit of E/E_{FG} at different temperatures are summarised in Table 1. A plot of E/E_{FG} in the continuum limit versus the temperature is shown in Fig. 3. As expected the energy per particle increases with increasing temperature. As for the chemical potential, we observe excellent agreement with experiment [8] and theory [9, 10] for sufficiently low temperatures.

3.3 The temperature dependence of the contact

The quantity called contact plays an important role for several universal relations derived by Tan [12]. It can be interpreted as a measure of the local pair density [13]. One possible definition is $C = m^2 g_0 E_{\mathrm{int}}$, where g_0 is the physical coupling constant [13, 14]. The contact density $\mathscr{C}$ is defined via $C = \int \mathscr{C}(\mathbf{r}) d^3 r$, or for homogeneous systems simply $C = \mathscr{C}V$. The dimensionless quantity $\mathscr{C}/\varepsilon_F^2 = \mathscr{C}/k_F^4$ can be expressed as $\mathscr{C}/\varepsilon_F^2 = (U E_{\mathrm{int}})/(4L^3\varepsilon_F^2)$ using lattice quantities.

In [15] we have presented preliminary results for the contact density at the critical point. Now we extend this study to other values of the temperature. For the finite-size scaling we can rewrite the dimensionless contact density as

$$\frac{\mathscr{C}}{\varepsilon_F^2} = \frac{U E_{\mathrm{int}}}{4L^3\varepsilon_F^2} = \frac{U}{4} \cdot \frac{E_{\mathrm{int}}}{L^3\nu} \cdot \frac{\nu}{\varepsilon_F^2} \propto \nu^{-1/3}(E_{\mathrm{int}}/N). \tag{3.3}$$

We have already seen that E/N is independent of L. Hence this part of the contact density can be averaged over the different lattice sizes, while the thermodynamic limit for the part proportional to $\nu^{-1/3}$ follows from the thermodynamic limit of the filling factor ν.

The fit results are listed in Table 1. Figure 4 shows the contact density versus the temperature in the continuum limit. Our result at the two lowest temperature values $T/T_c = 0.7$ and $T = T_c$
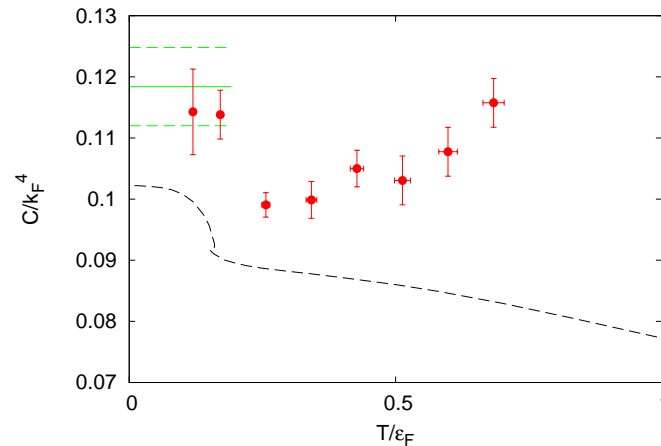
Figure 4: The contact density in the continuum limit versus the temperature. We compare our results (red circles) with results obtained with the Luttinger-Ward formalism [16] (black dashed line) and the experimental zero-temperature result [17] with the error margin (green lines).

show excellent agreement with the zero-temperature experimental result [17].

Acknowledgments

References

[1] R. Feynman, *Int. J. Theor. Phys.* **21**, 467-488 (1982).

[2] see e.g. S. Giorgini, L. P. Pitaevskii and S. Stringari, *Rev. Mod. Phys.* **80**, 1215-1274 (2008).

[3] O. Goulko, M. Wingate, *Phys. Rev. A* **82**, 053621, (2010).

[4] E. Burovski, N. Prokof'ev, B. Svistunov, M. Troyer, *New J. Phys.* **8**, 153 (2006).

[5] A. N. Rubtsov, V. V. Savkin, A. I. Lichtenstein, *Phys. Rev. B* **72**, 035122 (2005).

[6] O. Goulko, M. Wingate, `PoS(LAT2009)062`,`[arXiv:0910.3909]`.

[7] O. Goulko, Ph.D. thesis, University of Cambridge (2011).

[8] M. J. H. Ku, A. T. Sommer, L. W. Cheuk and M. W. Zwierlein, *Science* **335**, 563-567 (2012).

[9] K. Van Houcke, F. Werner, E. Kozik, N. Prokofev, B. Svistunov, M. Ku, A. Sommer, L. W. Cheuk, A. Schirotzek and M. W. Zwierlein, *Nature Physics* **8**, 366 (2012).

[10] R. Haussmann, W. Rantner, S. Cerrito, and W. Zwerger, *Phys. Rev. A* **75**, 023610 (2007).

[11] X.-J. Liu, H. Hu and P. D. Drummond, *Phys. Rev. Lett.* **102**, 160401 (2009).

[12] S. Tan, *Ann. Phys.* **323**, 2952 (2008); ibid 2971; ibid 2987.

[13] E. Braaten, `[arXiv:1008.2922]`.

[14] F. Werner, Y. Castin, `[arXiv:1001.0774]`.

[15] O. Goulko, M. Wingate, `PoS(LAT2010)187`,`[arXiv:1011.0312]`.

[16] T. Enss, R. Haussmann and W. Zwerger, *Annals Phys.* **326**, 770-796 (2011).

[17] N. Navon, S. Nascimbène, F. Chevy, C. Salomon, *Science* **328**, 729 (2010).